Electrochimica Acta 94 (2013) 49–56

Contents lists available at SciVerse ScienceDirect

Electrochimica Acta

journal homepage: www.elsevier.com/locate/electacta

Heterogeneous electron-transfer rate constants for ferrocene and ferrocene carboxylic acid at boron-doped diamond electrodes in a room temperature ionic liquid

Doo Young Kim[a,1], Ju Chan Yang[b], Hyoun Woo Kim[b], Greg M. Swain[a,*]

[a] Department of Chemistry, Michigan State University, East Lansing, MI 48824-1322, United States
[b] Division of Materials Science and Engineering, Hanyang University, Seoul 133-791, Republic of Korea

ARTICLE INFO

Article history:
Received 28 August 2012
Received in revised form 24 January 2013
Accepted 25 January 2013
Available online 4 February 2013

Keywords:
Diamond electrodes
Room temperature ionic liquids
Cyclic voltammetry
Electrode kinetics

ABSTRACT

Heterogeneous electron-transfer rate constants were determined for ferrocene and ferrocene carboxylic acid (FCA) in the room temperature ionic liquid (RTIL), 1-butyl-3-methylimidazolium tetrafluoroborate ($BMIMBF_4$), at boron-doped microcrystalline diamond thin-film electrodes. Comparison data for FCA in 1 M KCl were also obtained. The apparent heterogeneous electron-transfer rate constant, k^0_{app}, for FCA was 10× lower in the RTIL $1.5 (\pm 1.1) \times 10^{-3}$ cm s^{-1} as compared to KCl $4.6 (\pm 1.3) \times 10^{-2}$ cm s^{-1}. The k^0_{app} for ferrocene was also 10x lower in the RTIL $5.0 (\pm 1.2) \times 10^{-3}$ cm s^{-1} as compared to a common organic electrolyte solution $5.5 (\pm 1.2) \times 10^{-2}$ cm s^{-1}. The diffusion coefficient for FCA (D_{red}) was determined by chronoamperometry to be 1.3×10^{-7} cm^2 s^{-1}, ca. 100× lower than the value (1.9×10^{-5} cm^2 s^{-1}) in KCl. The lower diffusion coefficient is consistent with the 100× greater viscosity of the RTIL. The lower k^0_{app} values for these outer-sphere redox systems is attributed, at least in part, to a reduced number of attempts to surmount the activation barrier (i.e., a reduced nuclear frequency factor, ν_n) due to the more viscous medium.

1. Introduction

High quality, hydrogen-terminated diamond electrodes have attracted considerable attention in recent years due to some attractive electrochemical properties: (i) improved signal-to-background ratios in electroanalytical measurements due to a low and stable background current, (ii) resistance to electrode deactivation and fouling due to weak molecular adsorption, (iii) wide working potential window of ~3–4 V in aqueous electrolytes, (iv) excellent microstructural and morphological stability at extreme anodic and cathodic potentials and or high current densities (1–10 A cm^{-2}), and (v) good electrode responsiveness with relatively rapid electrode kinetics for multiple dissolved redox systems without conventional pretreatment [1–4].

Several factors influence the electrochemical activity (i.e., electrode reaction kinetics) of boron-doped diamond electrodes: (i) potential-dependent density of electronic states, (ii) dopant type, level, and distribution, (iii) surface chemistry, (iv) morphology and microstructure, (v) defect density, (vi) adventitious nondiamond sp^2 carbon impurity content, and (vii) the double layer structure. The extent to which these factors affect the electrochemical activity strongly depends on the reaction mechanism of the particular redox system. By choosing the appropriate growth conditions, the film quality and corresponding electrode behavior can be controlled. Several papers have reported on the structure-function relationships and electrochemical kinetics of diamond electrodes in conventional aqueous and organic electrolytes [1–8]. However, there has been little work reported about these relationships in ionic liquid media [9].

Room temperature ionic liquids (RTILs) are emerging as a new electrolytes for electrochemical measurements and processes. RTILs are distinct from aqueous electrolyte solutions because they contain no solvent. They are salts in the liquid phasecomposed of bulky cations and anions of unequal size [10–15]. RTILs have received attention by electrochemists because of several attractive properties: high thermal and chemical stability, low vapor pressure, non-flammability, high ionic conductivity and high breakdown potential [10–15]. Because of the low vapor pressure and wide potential window, RTILs are being utilized more and more in electrochemical applications, including energy storage devices [16–18]. The ions of an RTIL are not solvated like they are in aqueous electrolyte solutions. This means that the electric double layer formed should be structurally distinct from that formed in an aqueous electrolyte. In other words, the Gouy–Chapman–Stern model

* Corresponding author. Tel.: +1 517 355 9715x229; fax: +1 517 353 1793.
E-mail address: swain@chemistry.msu.edu (G.M. Swain).
[1] Present address: Department of Chemistry, University of Kentucky, Lexington, KY, United States.

0013-4686/$ – see front matter © 2013 Elsevier Ltd. All rights reserved.
http://dx.doi.org/10.1016/j.electacta.2013.01.140

that is typically used to describe the interfacial structure in aqueous electrolyte solutions likely inaccurately describes the interfacial organization of an RTIL. Our group is interested in the interfacial structure formed at boron-doped diamond electrodes in various electrolyte solutions and how the electrolyte composition affects heterogeneous electron-transfer rate constants [19]. RTILs constitute a relatively unstudied medium.

There have been a few reports so far describing the basic electrochemical properties of different solid electrodes or the heterogeneous electron-transfer kinetics of various redox analytes in RTILs [13,20–25]. Barrosse-Antle et al. reported background cyclic voltammetric *i–E* curves and working potential windows for Pt, Au, GC, and boron-doped diamond in several amine-based RTILs [15]. Compton et al. reported heterogeneous electron-transfer rate constants, k^0, for ferrocene derivatives in 1-ethyl-3-methylimidazolium bis(trifluoromethylsulfonyl) imide at a Pt microband electrode [25]. k^0 varied from ~0.1–0.2 cm s^{-1}, and was 5–10× lower than the rate constants in acetonitrile (CH_3CN). Tachikawa et al. reported on the electrode kinetics of ferrocene in amide-based RTILs at Pt [26]. k^0 ranged from 0.2–1.5 × 10^{-2} cm s^{-1}, and was 2–3 orders of magnitude lower than the value in CH_3CN. Similarly, Hapiot et al. also found that k^0 values for ferrocene and anthracene are ~1–2 orders of magnitude lower in amine- or imidazolium-based ionic liquids than in CH_3CN [27]. The lower k^0 values in RTILs are attributed, in part, to the higher viscosity, hence the lower diffusion coefficient for the redox system in the medium [13,15,23,25–27]. This causes a reduced number of attempts to surmount the activation barrier, leading to the lower k^0.

Compared to the number of studies at metal electrode, reports for carbon electrodes in RTILs are far fewer in number, especially for sp^3-bonded diamond electrodes, with most of the reported work involving capacitance measurements [13,23,28–30]. Some understanding of structure-function relationships at diamond electrodes now exists for aqueous and non-aqueous electrolytes [1–8,31,32]; however, little information is available for RTILs. In the present study, we report on the heterogeneous electron-transfer rate constants for ferrocene and ferrocene carboxylic acid (FCA) in the room temperature ionic liquid (RTIL), 1-butyl-3-methylimidazolium tetrafluoroborate ($BMIMBF_4$), at boron-doped microcrystalline diamond thin-film electrodes. We selected this RTIL simply because it was readily available while the polycrystalline diamond electrodes were used because of our extensive past work with them in aqueous and nonaqueous electrolyte solutions. Ferrocene and FCA were selected as test systems because they exhibit electrochemical behavior reflective of an outer-sphere redox couple, without complications arising from adsorption or bond breakage/formation [23,25,27,33].

2. Experimental

2.1. Electrode fabrication

The boron-doped diamond thin films were deposited on an electrically conducting p-Si (1 0 0) substrate (~10^{-3} Ω cm, Virginia Semiconductor Inc., Fredericksburg, VA) using microwave-assisted chemical vapor deposition (CVD). The CVD reactor was 1.5 kW, 2.54 GHz commercial system (Seki Technotron Corp., Japan) with a 1 L quartz bell jar. The Si substrate was pretreated by mechanically scratching with 1 μm diameter diamond powder (GE Superabrasives, Worthington, OH) on a felt polishing pad. The scratched substrate was then sequentially rinsed with ultrapure water, isopropyl alcohol (IPA), acetone, IPA, and finally ultrapure water to remove polishing debris from the surface. The striations and embedded diamond powder particles introduced by the scratching serve as the initial diamond nucleation sites.

High quality (continuous polycrystalline films with little sp^2 non-diamond carbon impurity) microcrystalline diamond thin films were deposited using a methane/hydrogen (C/H) source gas mixture at a volumetric ratio of 0.5%, a total gas flow of 200 sccm, a plasma power of 1000 W, a system pressure of 45 Torr, and a substrate temperature near 750 °C. Ultrahigh purity (99.999%) methane and hydrogen were used. 10 ppm of B_2H_6 was introduced for boron-doping. The growth time was 10 h. At the end of the growth period, the CH_4 and B_2H_6 gas flows were stopped and the film remained exposed to a hydrogen plasma for 10 min at the deposition conditions. The plasma power and pressure were then slowly reduced to 400 W and 20 Torr over the next 25 min to cool the sample to less than 400 °C in the presence of atomic hydrogen. This step is important for maintaining a hydrogen-terminated surface. The resulting films possessed a continuous, faceted morphology with a nominal crystallite size of 0.5–1 μm. A predominance of (1 0 0) and (1 1 1) crystal faces were exposed. The nominal boron-doping level was >1 × 10^{21} cm^{-3} producing an electrical resistivity of <0.01 Ω cm, based on boron nuclear reaction and electrical measurements of other films grown under identical conditions. Raman spectra consisted of a sharp one-phonon diamond line at 1330–1332 cm^{-1} along with very weak scattering intensity between 1510 and 1550 cm^{-1} due to low levels of sp^2-bonded carbon impurity (Refs. [3–6] therein]. Two peaks were also present at ca. 550 and 1200 cm^{-1}. These bands are characteristic of heavily doped films and likely arise from scattering by impurity-induced electronic states. It is important to note that the electronic properties of polycrystalline diamond are influenced by the boron-doping level as well as the hydrogen content, intrinsic defects and different structural features.

If the films were not used immediately after growth, they were chemically treated to clean the surface. First, they were immersed in warm (~50 °C) 1:3 HNO_3:HCl (v/v) for 30 min. The films were then rinsed in ultrapure H_2O and dried. Second, the films were exposed to warm 30% H_2O_2 (Sigma–Aldrich) for 30 min followed by a thorough rinse with ultrapure water. The chemically-treated films (oxygen terminated) were then hydrogen-plasma treated at ~750 °C, 40 Torr and 1000 W for 30 min to remove surface oxygen and rehydrogenate the surface. After plasma treatment, the samples were slowly cooled in the presence of atomic hydrogen, as described above. We have found that this treatment is also effective at activating poorly responding diamond electrodes with extensive past histories [33].

2.2. Characterization by scanning electron microscopy (SEM) and Raman spectroscopy

The diamond film morphology was characterized by field-emission scanning electron microscopy (JSM-6300F, JEOL, Ltd., Tokyo, Japan). The crystallinity, carbon phase purity, and microstructure of the film were evaluated by Raman spectroscopy. The spectra were acquired at room temperature using a Spex 1250 spectrograph with a 600 groove/mm holographic grating (Horiba Jobin-Yvon). The 514.5 nm line from an argon ion laser (Melles Griot CV) was used for excitation. The detector was a Symphony 2000 × 800 CCD (Horiba Jobin-Yvon) with a pixel size of 15 μm.

2.3. Electrochemical measurements

Cyclic voltammetric measurements were carried out in a single compartment glass cell using a CHI potentiostat (Model 660D, Austin, TX). Potential sweep rates from 10 to 200 mV s^{-1} were used. For the measurements in aqueous electrolyte, a homemade Ag/AgCl reference electrode, filled with 3 M KCl (0.197 V vs. NHE), and a graphite rod counter electrode were employed. All potentials

in aqueous media are reported versus this reference. In the RTIL, a Ag QRE was substituted as the reference. Identical voltammetric features were found when using a Ag/AgCl (3 M KCl) reference electrode placed in a cracked-glass Luggin capillary filled with the $BMIMBF_4$ ionic liquid. This arrangement was employed to minimize water contamination of the main solution. The potential of the Ag QRE in 1 M KCl was −0.072 V vs. Ag/AgCl (3 M KCl) and in the $BMIMBF_4$ was 0.120 V vs. Ag/AgCl (3 M KCl). In the electrochemical cell, an O-ring defined the geometric area (0.2 cm^2) with all currents reported being normalized to this area. The electrolyte was either 1 M KCl (99.999%, Aldrich) or the ionic liquid, $BMIMBF_4$ (>98.5% HPLC Grade, ≤500 ppm H_2O, Sigma–Aldrich).

The voltammetric measurements were made with the cell placed inside of an N_2-purged dry box (Coy Laboratories, MI) with a 0% relative humidity, as measured with a hygrometer. To perform a measurement with the ionic liquid, the electrochemical cell was placed in the dry box. The cell was flushed with N_2 before being filled with the ionic liquid. The solution was then purged with Ar for 20 min [34]. During a measurement, a blanket of N_2 covered the solution. No measurement was made to quantify the water content after purification.

Chronoamperometry was performed to determine the diffusion coefficient (D_{red}) of ferrocene carboxylic acid (FCA) in the two electrolytes (1 M KCl and $BMIMBF_4$). For 1 M KCl, the potential was stepped from 0 to 0.6 V vs. Ag/AgCl, and held at this potential for 5 s to measure the faradaic current due to the oxidation of FCA to FCA^+. For $BMIMBF_4$, the potential was stepped from 0 to 0.9 V vs. Ag QRE and held at this potential for 5 s to measure the oxidation current. After background correction, the measured faradaic currents were analyzed using the Cottrell equation. The calculated D value for FCA was 1.9×10^{-5} cm^2 s^{-1} in 1 M KCl and 1.3×10^{-7} cm^2 s^{-1} in $BMIMBF_4$. Due to a higher viscosity, the diffusion coefficient in the RTIL is 100× less than the value in aqueous media. By way of comparison, reported literature values of D_{red} for ferrocene and ferrocene carboxylic acid (FCA) in the ionic liquid, 1-ethyl-3-methylimidazolium bis(trifluoromethylsulfonyl) imide, are 6.5×10^{-7} and 2.6×10^{-7} cm^2 s^{-1}, respectively [23,26]. It should be noted that D_{red} values for ferrocene or FCA are not equal to their D_{ox} values for in RTILs. For example, Rogers et al. have reported a D_{red} of 1.8×10^{-7} cm^2 s^{-1} for ferrocene (FC) in $BMIMBF_4$ and a D_{ox} of 1.3×10^{-7} cm^2 s^{-1} for ferrocenium (Fc^+) [34] ($D_{Fc+}/D_{Fc} = 0.72$). In our work, we found the D_{red} for FCA in $BMIMBF_4$ to be 1.3×10^{-7} cm^2 s^{-1}, as mentioned above, and through digital simulation D_{ox} was determined to be 8.5×10^{-8} cm^2 s^{-1} ($D_{FCA+}/D_{FCA} = 0.65$).

The apparent heterogeneous electron-transfer rate constants, k^0_{app}, were determined by cyclic voltammetry using peak potential separation vs. scan rate ($\Delta E_p - \upsilon$) data analyzed by the Nicholson method [35,36]. k^0_{app} values were calculated from voltammetric data at five scan rates (100–500 mV s^{-1}). In this approach, one determines the variation of ΔE_p with υ, and from this variation, ψ. From ψ, one can calculate k^0 according to the following equation:

$$\Psi = \frac{\{(D_o/D_r)^{a/2} k^0\}}{(\pi D_o f \upsilon)^{1/2}} \quad (1)$$

where $f = F/RT$ (F = Faraday constant; R = gas constant; T = temperature (K)) and υ (V s^{-1}) is the scan rate. With voltammetric methods, one must verify that any uncompensated resistance, R_u, is small meaning that ohmic effects contribute negligibly to the ΔE_p values [36,37]. We verified this by recording ΔE_p values at a single scan rate as a function of the redox analyte concentration (0.1–1 mM). We found that the ΔE_p for FCA was independent of the concentration at the different scan rates, as expected if ohmic resistance effects are negligible. Fitting the experimental cyclic voltammetric i–E curves to the simulated ones using BAS DigiSim™ simulator software (3.0) was used to validate the calculated k^0_{app}. No correction for double layer effects (so-called Frumkin correction) was made so we refer to the rate constants as apparent.

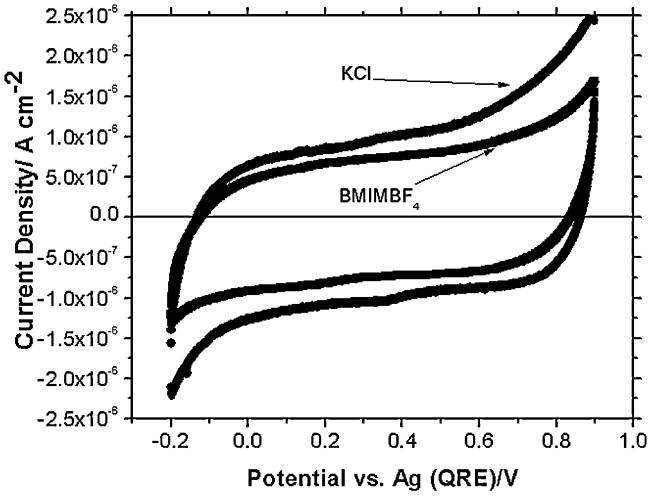

Fig. 1. Comparison of background cyclic voltammetric i–E curves for a boron-doped diamond thin-film electrode in 1 M KCl and $BMIMBF_4$ at 50 mV s^{-1}. The $BMIMBF_4$ was purified by heating in vacuum (80 °C) overnight and storage over activated molecular sieves (5 Å).

2.4. Reagents

Ferrocene carboxylic acid and ferrocene (Sigma–Aldrich, St. Louis, MO) were used without any additional purification. The acetonitrile (Merck, HPLC grade) was distilled and stored over activated molecular sieves (5 Å). The sodium and tetrabutylammonium perchlorate salts (Sigma–Aldrich) were used as received. $BMIMBF_4$ (Sigma–Aldrich) is hygroscopic so to minimize water contamination, the ionic liquid was dried under vacuum for 24 h at 80 °C and then stored over activated (heat treated at 400 °C in a furnace) 5 Å molecular sieves. The dehydrated RTIL was tightly sealed and kept in the dry box. In $BMIMBF_4$, the midpoint potential for the ferrocene/ferrocenium couple was 0.34 V vs. Ag QRE and 0.46 V vs. Ag/AgCl.

3. Results

Fig. 1 presents background cyclic voltammetric i–E curves for a boron-doped diamond thin-film electrode in 1 M KCl and $BMIMBF_4$. The scan rate was 50 mV s^{-1} and the scans shown are the 10th cycle. The curves are both featureless (no peaks) within the potential window. The current for the RTIL is 1–2× lower than the current for KCl over most of the potential range. The lower current is consistent with a lower capacitance, C_{dl}. For both electrolytes, the curves were unchanged in shape with cycle number. Further evidence of the stability of the diamond-RTIL interface was the constant open circuit potential of 0.225 V vs. Ag (QRE) measured over a 15 min period at the beginning of the measurements.

Fig. 2A and B show a series of cyclic voltammograms at a diamond thin-film electrode at increasing scan rate from 10–200 mV s^{-1} in (A) $BMIMBF_4$ and (B) 1 M KCl. In both electrolytes, the background cyclic voltammograms are featureless within the potential ranged probed with currents that increase proportionally with the scan rate. For example, the anodic current (i_a) at 0.4 V increased linearly with the scan rate at both electrodes with a linear regression correlation coefficient of 0.9842 for the RTIL and 0.9989 for KCl. The curve shapes were unchanged with cycle

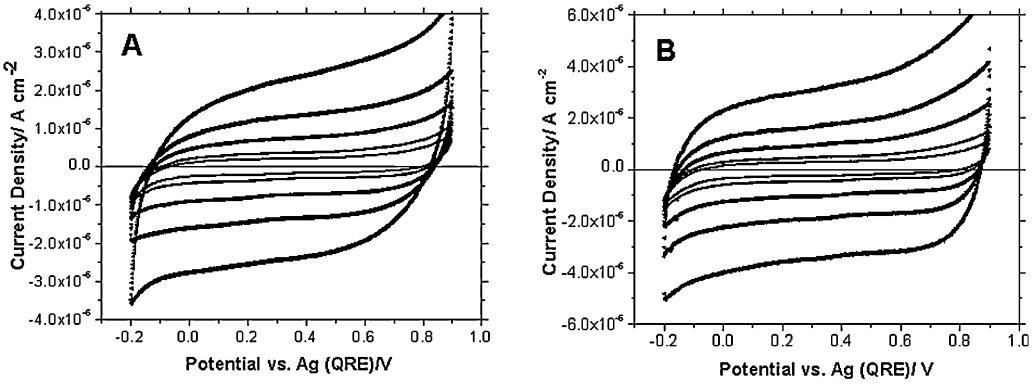

Fig. 2. Background cyclic voltammetric *i–E* curves for a boron-doped diamond thin-film electrode as a function of the scan rate in (A) $BMIMBF_4$ and (B) 1 M KCl. Scan rates of 10, 20, 50, 100 and 200 mV s^{-1} were employed. The $BMIMBF_4$ was purified by heating in vacuum (80 °C) overnight and storage over activated molecular sieves (5 Å).

number (5–10) in both media. Assuming the current is purely capacitive, the following relationship holds

$$i_{a,c} = AC_{dl}\upsilon \quad (2)$$

where A is the electrode area (cm^2). C_{dl} can be calculated from the slope of a plot of $i_{a,c}$ vs. υ. The calculated C_{dl} of the diamond electrode at 0.4 V was 10.9 and 15.1 μF cm^{-2}, respectively, in the RTIL and 1 M KCl. These values are similar to those reported for KCl and ionic liquids of different composition to the one used in our work [23].

Fig. 3 shows a background cyclic voltammogram for a diamond thin-film electrode in $BMIMBF_4$ over a wider potential range. A small anodic peak is seen at about 1 V prior to the onset of larger anodic current. The origin of this peak is unknown. The anodic current at the positive limit is presumed to be due to the oxidation of the RTIL. A weak cathodic peak is seen at about −1 V just prior to the onset of a larger cathodic current. The cathodic current in this potential region is likely contributed to by the reduction of dissolved O_2 not fully removed by the Ar gas purge. This is based on the observation that this current increased if the RTIL was not deoxygenated. The larger cathodic current at −2 V is presumed to be due to reduction of the RTIL cation. Using the limits of ±40 μA cm^{-2}, the working potential window is 3.6 V. This wide window is characteristic of boron-doped diamond electrodes and is larger than the windows reported for other protic ionic liquids [23]. Our potential window is less than the 4.7 V (larger current density limits) reported by Barrosse-Antle et al. for $BMIMBF_4$ at a Pt microdisc electrode [15]. Additional work is needed to better understand the redox reactions that contribute to working potential window for diamond electrodes when in contact with this and other RTILs. Based on the wide potential window, we suppose that the voltammogram in Fig. 3 is reflective of a relatively pure RTIL low in H_2O content.

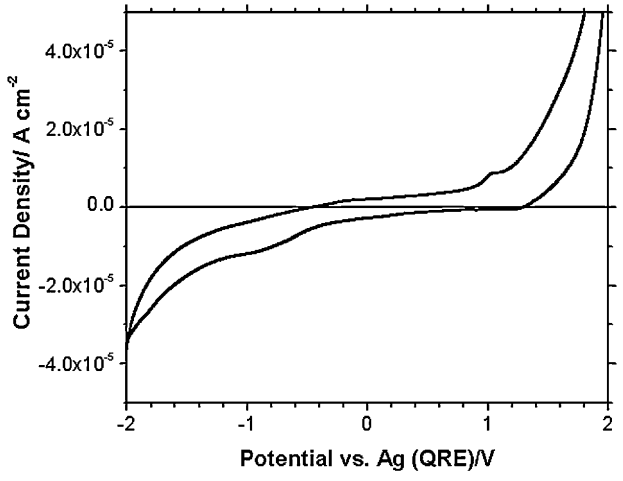

Fig. 3. Background cyclic voltammetric *i–E* curve for a boron-doped diamond thin-film electrode in $BMIMBF_4$ showing the working potential window. Scan rate = 50 mV s^{-1}. The $BMIMBF_4$ was purified by heating in vacuum (80 °C) overnight and storage over activated molecular sieves (5 Å).

The diffusion coefficient for ferrocene carboxylic acid (FCA) in the two media was determined by chronoamperometry. Current–time profiles are shown in Fig. 4A. Values of 1.3×10^{-7} cm^2 s^{-1} in $BMIMBF_4$ and 1.9×10^{-5} cm^2 s^{-1} in KCl were determined for D_{red} from Cottrell analysis of the faradaic current–time response. The oxidation of FCA involves the one-electron transfer to form the ferrocenium ion (FCA^+), and at the applied potential of 0.6 V vs. Ag/AgCl (3 M KCl) and 0.9 V vs. Ag QRE ($BMIMBF_4$), the current is diffusion limited. Plots of i_f vs. $t^{-1/2}$ were linear, indicative of a reaction rate limited by semi-linear diffusion (Fig. 4B). As mentioned above, the diffusion coefficients (D_{red}) were calculated as 1.9×10^{-5} cm^2 s^{-1} in 1 M KCl and 1.3×10^{-7} cm^2 s^{-1} in $BMIMBF_4$. The fact that the FCA diffusion coefficient in the RTIL is 100× less is consistent with the 100× greater viscosity of the ionic liquid ($BMIMBF_4$, η = 112 cp) [34] compared to H_2O and indicates that the RTIL is low in water impurity.

Fig. 5A shows a cyclic voltammetric *i–E* curve for 0.1 mM FCA in 1 KCl. A simulated curve is shown, for comparison. The scan rate was 100 mV s^{-1}. The simulated curve was generated using $D_{red} = 1.9 \times 10^{-5}$ cm^2 s^{-1} and assuming $D_{ox} = D_{red}$. A well-defined voltammetric response is observed with a peak potential separation, ΔE_p, of 68 mV, an $E_{p/2}$ of 0.310 V, and a peak current ratio, i_p^a/i_p^c of 1. The oxidation peak current varied linearly with the square root of the scan rate (R^2 = 0.9982) between 10 and 200 mV s^{-1}, as shown in Fig. 5C. This indicates the oxidation reaction rate is controlled by semi-infinite linear diffusion of FCA to the electrode surface. The simulated curve at this scan rate matches well the experimental curve. Fig. 5B presents a cyclic voltammetric *i–E* curve measured for 1 mM FCA in $BMIMBF_4$. The potential is reported versus the midpoint potential of the ferrocene/ferrocenium (Fc/Fc^+) couple. The scan rate was 100 mV s^{-1}. The simulation was performed using $D_{red} = 1.3 \times 10^{-7}$ cm^2 s^{-1} and $D_{ox} = 8.5 \times 10^{-8}$ cm^2 s^{-1}. In $BMIMBF_4$, like in KCl, a well-defined voltammetric response was observed with a ΔE_p of 75 mV, an $E_{p/2}$ of 0.146 V and an i_p^a/i_p^c ratio >1. The greater than unity ratio is consistent with the differences in diffusion coefficients for the two halves of the redox couple [25]. As shown in Fig. 5D, the oxidation peak current varied linearly with the square root of the scan rate (R^2 = 0.9892) between 10 and 200 mV s^{-1}, consistent with a reaction rate limited by semi-infinite linear diffusion. In both media, ΔE_p increased progressively between 100 and 500 mV s^{-1} indicative of quasi-reversible electrochemical reaction kinetics.

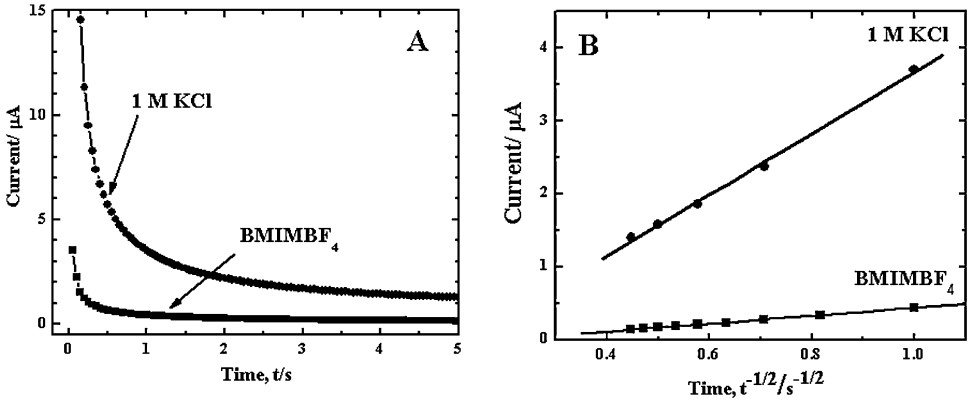

Fig. 4. (A) Chronoamperometric *i–t* profiles for the diffusion-limited oxidation of 0.1 mM FCA in 1 M KCl and $BMIMBF_4$. The potential was stepped from 0 to 0.6 V vs. Ag/AgCl for KCl and from 0.3 to 0.9 V vs. Ag QRE for $BMIMBF_4$. (B) Corresponding plots of i_f vs. $t^{-1/2}$ calculated from current–time curves. i_f values were determined via background subtraction. The $BMIMBF_4$ was purified by storage over activated molecular sieves (5 Å).

When using cyclic voltammetric $\Delta E_p - \upsilon$ trends to determine heterogeneous electron-transfer rate constants [36,37], one needs to verify that ohmic effects are not influencing the curve shapes. This was done by measuring the peak potentials at a given scan rate between 100 and 500 mV s^{-1} as a function of the FCA solution concentration (0.1–1 mM) in both 1 M KCl and $BMIMBF_4$. In both media, the peak currents increased linearly with the redox analyte concentration at a fixed scan rate. Furthermore, the peak positions at a given scan rate were independent of the redox analyte concentration in both media. These trends confirm that the $\Delta Ep - \upsilon$ relationships were controlled primarily by the electrode kinetics and not by ohmic resistance effects. The simulation results validate the experimentally determined k^0_{app} values. The Nicholson treatment relates ΔE_p to the dimensionless kinetic parameter, Ψ and is useful for determining rate constants of redox systems with cyclic voltammetric peak separations in the range of 65–200 mV [36]. Analysis of our data, summarized in Table 1, reveal k^0_{app} values for FCA in $BMIMBF_4$ of 3.0 ($\pm$1.1) $\times 10^{-3}$ cm s^{-1} and in KCl of 4.6 ($\pm$1.3) $\times 10^{-2}$ ($n \geq 3$ diamond electrodes). These data are presented in Table 1. A similar 10$\times$ lower k^0_{app} is seen for ferrocene in the RTIL 5.0 ($\pm$1.2) $\times 10^{-3}$ cm s^{-1}) as compared to the organic electrolyte 5.5 ($\pm$1.2) $\times 10^{-2}$ cm s^{-1}.

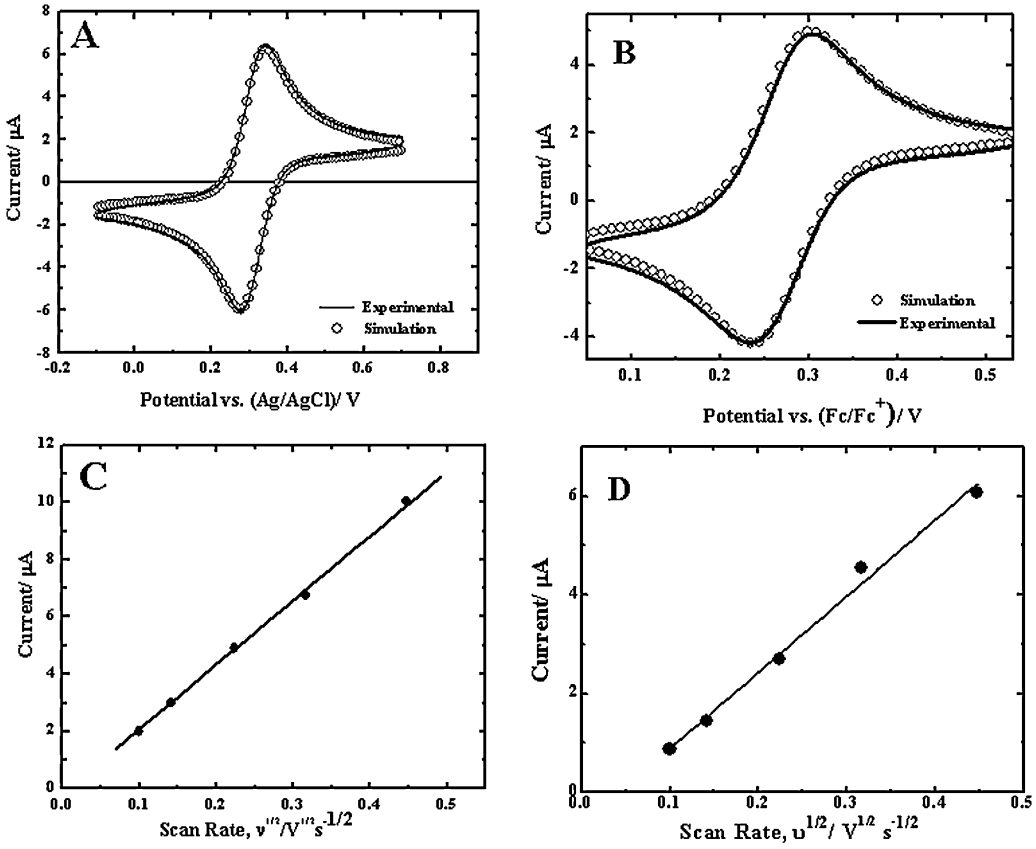

Fig. 5. Cyclic voltammetric *i–E* curves for (A) 0.1 mM FCA in 1 M KCl and (B) 1 mM FCA in $BMIMBF_4$ at a boron-doped diamond thin-film electrode. Experimental and simulated (DIGISIM™) curves are presented for comparison. Scan rate = 100 mV s^{-1}. i_p–$\nu^{1/2}$ plots to demonstrate diffusion-controlled kinetics are shown for (C) 0.1 mM FCA in 1 M KCl and (D) 1 mM FCA in $BMIMBF_4$. Data plotted for scan rates of 100–500 mV s^{-1}. The $BMIMBF_4$ was purified by storage over activated molecular sieves (5 Å).

Table 1
The medium viscosity (η), diffusion coefficients (D), and heterogeneous rate constant (k^2_{app}), for ferrocene and ferrocene carboxylic acid (FCA) in different media at boron-doped diamond, Pt, and glassy carbon electrodes.

Redox analyte in electrolyte/solvent	Electrode	η (mPa s)	D_{red} ($cm^2\ s^{-1}$)	k^o_{app} ($cm\ s^{-1}$)[a]	Reference
FCA in 1 M KCl	Diamond	1	1.9×10^{-5}	$4.6\ (\pm 1.3) \times 10^{-2}$	This work
FCA in $BMIMBF_4$	Diamond	112	1.3×10^{-7}	$1.5\ (\pm 1.1) \times 10^{-3}$	This work
Ferrocene in $BMIMBF_4$	Diamond	112	2.2×10^{-7}	$5.0\ (\pm 1.2) \times 10^{-3}$	This work
Ferrocene in PP13-TFSA	Pt	129	1.6×10^{-7}	$2.3\ (\pm 1.1) \times 10^{-3}$	[26]
Ferrocene in $BMIMPF_6$	Glassy carbon	308	0.59×10^{-7}	2.3×10^{-4}	[45]
Ferrocene in 0.1 M $NaClO_4/CH_3CN$	Diamond	0.38	2.4×10^{-5}[b]	$5.5\ (\pm 1.2) \times 10^{-2}$ $4.2\ (\pm 1.5) \times 10^{-2}$[b]	This work
Ferrocene in 0.1 M $TBAClO_4/CH_3CN$	Diamond	0.38	2.4×10^{-5}[b]	$5.8\ (\pm 1.6) \times 10^{-2}$ $4.8\ (\pm 1.5) \times 10^{-2}$[b]	This work

[a] Transfer coefficient of $\alpha = 0.5$ used in the calculation of the rate constants. Rate constants were determined at a 0.1 mM redox analyte concentration, and are reported as a average ± standard deviation. The latter is the variability in rate constant determined by the Nicholson treatment ($\Delta Ep - \upsilon$ trends) at scan rates from 20 to 200 mV s^{-1}. Both ferrocene and FCA behaved quasi-reversibly at these scan rates.
[b] Diffusion coefficient was taken from Ref. [32]. $BMIMBF_4$ = 1-butyl-3-methylimidazolium tetrafluoroborate. $BMIMPF_6$ = 1-butyl-3-methylimidazolium hexafluorophosphate. PP13-TFSA = *N*-methyl-*N*-propylpiperidinium bis(trifluoromethanesulfonyl) amide. $TBAClO_4$ = tetrabutylammonium perchlorate.

4. Discussion

Our results indicate that the heterogeneous electron-transfer rate constants for ferrocene and FCA in the RTIL are approximately 10× lower than the values in conventional aqueous or non-aqueous solvent/electrolyte systems (see Table 1). In order to understand the cause(s) for the more sluggish kinetics, there are at least two factors to consider. The first is the higher viscosity of the RTIL, as compared to aqueous or nonaqueous electrolyte solutions. $BMIMBF_4$ is 100× more viscous than a KCl solution. The more viscous RTIL means that the diffusion coefficient for FCA, or any redox molecule for that matter, will be lower. This is apparent when considering the Stokes–Einstein equation [38]:

$$D = \frac{k_B T}{6\pi a \eta} \tag{3}$$

The diffusion coefficient (D_{red}) for FCA was found to be $1.3 \times 10^{-7}\ cm^2\ s^{-1}$ in $BIMBF_4$ and $1.9 \times 10^{-5}\ cm^2\ s^{-1}$ in KCl. This difference is a factor of 100, consistent with the viscosity difference. Water impurity in RTILs tends to decrease the viscosity and increase the conductivity (Refs. [13,15] therein). The presence of water will narrow the potential window and increase the diffusion coefficient of dissolved redox species due to a lowering of the viscosity. Even though we made no measurement of the water content in the purified $BMIMBF_4$, the fact that the diffusion coefficient of FCA is 100× less than in KCl, consistent with the 100× viscosity difference, is a good indication that the water content in our RTIL was low. When working with RTILs, such as $BMIMBF_4$, one must be careful to minimize H_2O contamination.

The lower diffusion coefficient in $BMIMBF_4$ has a profound effect on the shape of both the kinetically- and diffusion-controlled regions of the cyclic voltammograms. Of course, the diffusion-limited current is lower in the RTIL. The higher viscosity (η) also affects the kinetically-controlled current by decreasing k^0. Tachikawa et al. have shown an inverse correlation between k^0 for ferrocene and η (viscosity) [26]. The Marcus expression for the heterogeneous electron-transfer rate constant of a redox molecule in an aqueous electrolyte is given as [26,39,40]:

$$k^0 = K_p k_{el} \upsilon_n \exp\left(\frac{-\Delta G^{\dagger}}{RT}\right) \tag{4}$$

where $\Delta G^{\ddagger}$ is the Gibbs activation energy, K_p is the precursor equilibrium constant, κ_{el} is the electronic transmission coefficient and υ_n is the nuclear frequency factor. R and T are the ideal gas constant and the temperature, respectively. The relationship indicates a direct proportionality between k^0 and the nuclear frequency factor, υ_n. The nuclear frequency factor is the effective frequency of passing through the transition state and the dynamics of this process are inversely related to the viscosity of the electrolyte solution, $\upsilon_n \propto 1/\eta$ [26]. More generally, k_{et} is determined by the collision frequency of a redox molecule with the electrode surface and the probability of electron transfer per collision ($k_{et} = \nu P_{et}$) [41]. As described by White and White, when a molecule arrives at the electrode surface via diffusion, it will make many collisions with the electrode surface before wandering off into the bulk solution [41]. During these "collisions", the molecule has many opportunities to donate or accept an electron. The take-home message is that diffusion as well as the collisions between a redox molecule and the electrode surface result from random motion. Both are more restricted in the more viscous RTIL. If the nuclear frequency factor were the only factor affected, then one would expect k^0_{app} values to be different by 100×, not the ca. 10× difference observed. This suggests that other parameters in the kinetic expression are affected by the properties of the RTIL.

Assuming the Marcus relationship expression appropriately describes k^0 in an RTIL, we suppose this decrease in υ_n may be offset by a reduced free energy of activation, $\Delta G^{\ddagger}$, for the electron transfer. Specifically, it seems possible the solvent reorganization energy might be less in the RTIL. Simply put, forming a positively charged FCA^+ or ferrocenium ion in the sea of bulky organic cations and counterbalancing anions might require less solution reorganization than would be the case in an aqueous electrolyte, specifically with regard to the organization of the solvating water molecules. In other words, one can envision placing a charged redox species in an RTIL with minimal restructuring of the local organic cations and anions. As pointed out by Fietkau et al. [25], the Marcus treatment is based on reorganization of solvent dipoles and this process is inapplicable in RTILs where the solvent is formed of ions. There is clearly a need for theoretical and experimental work to establish the criteria for outer-sphere electron transfer in RTILs [25]. While it remains to be tested, that the pre-exponential factor, A (specifically the nuclear frequency factor, υ_n), will be lower in the RTIL due to the lower analyte diffusion coefficient and that the $\Delta G^{\ddagger}$ will be lower in the RTIL due to a reduced solvent reorganization energy. For this reason, k^0_{app} is only 10× rather than 100× lower.

Two final points are worth mentioning. First, in general, our k^0_{app} values for ferrocene and FCA in the RTIL at diamond are 10–100× lower than are the values reported for other RTILs at various metal electrodes (Au and Pt) [23,25]. The more sluggish kinetics at diamond are likely due to the semi-metallic electronic properties of the material that translate into a lower potential-dependent density of electronic states as compared to metals. The second point, relevant for electron transfer in both aqueous/non-aqueous electrolytes and RTILs, is the variable electronic properties that exist across the diamond film surface. Boron-doping of diamond is inhomogeneous with certain growth sectors incorporating more boron than others. This leads to a film that is characterized by highly conducting regions isolated by less conducting zones. CP-AFM and SECM data

have clearly shown this [42–44]. The consequence of this is that the capacitance and cyclic voltammetric measurements reflect an ensemble average of the response of all the conducting and less conducting regions. This likely a cause for the lower background voltammetric current and capacitance, as compared to other metal and carbon electrodes. The redox reaction current mainly flows through the more conductive zones (so-called hot spots) leading to high local current densities.

5. Conclusions

The electron-transfer kinetics for ferrocene and ferrocene carboxylic acid (FCA) were investigated in the room-temperature ionic liquid, $BMIMBF_4$, at boron-doped diamond thin-film electrodes. Comparison measurements were made in either KCl or $NaClO_4/CH_3CN$. The apparent heterogeneous electron-transfer rate constant, k^0_{app}, for FCA was 10× lower in $BMIMBF_4$ ($1.5\ (\pm1.1)\times10^{-3}$ cm s^{-1}) as compared to KCl ($4.6\ (\pm1.3)\times10^{-2}$ cm s^{-1}). In a similar manner, k^0_{app} for ferrocene was 10x lower in the RTIL ($5.0\ (\pm1.2)\times10^{-3}$ cm s^{-1}) compared to previously reported data for $NaClO_4/CH_3CN$ ($4.2\ (\pm1.2)\times10^{-2}$ cm × s^{-1}) [32]. The diffusion coefficient (D_{red}) for FCA in $BMIMBF_4$ was determined to be 1.3×10^{-7} cm^2 s^{-1}, which is ca. 100× lower than the 1.9×10^{-5} cm^2 s^{-1} value in KCl. The 100× lower diffusion coefficient is consistent with the 100× greater viscosity of the RTIL. The higher viscosity of $BMIMBF_4$ reduces the nuclear frequency factor, υ_n (i.e., reduced number of attempts to surmount the activation barrier), which leads to a lower k^0_{app} value than is observed in aqueous media. If this were the only kinetic factor affected, then one would predict rate constants lower by a factor of 100, not 10×. Therefore, we suppose the decrease in υ_n is offset by a reduced activation barrier, $\Delta G^{\ddagger}$, for the electron transfer in the RTIL.

Acknowledgements

This work was generously supported by grants from the Army Research Office (W911NF-09-1-0451) and the Natural Science Foundation (CHE-0911383). The authors thank Yan Zhu for her assistance performing some of the cyclic voltammetric measurements.

References

[1] M.C. Granger, J. Xu, J.W. Strojek, G.M. Swain, Polycrystalline diamond electrodes: basic properties and applications as amperometric detectors in flow injection analysis and liquid chromatography, Analytica Chimica Acta 397 (1999) 145.
[2] M.C. Granger, M. Witek, J. Xu, J. Wang, M. Hupert, A. Hanks, M.D. Koppang, J.E. Butler, G. Lucazeau, M. Mermoux, J.W. Strojek, G.M. Swain, Standard electrochemical behavior of high-quality, boron-doped polycrystalline diamond thin-film electrodes, Analytical Chemistry 72 (2000) 3793.
[3] Y. Show, M.A. Witek, P. Sonthalia, G.M. Swain, Characterization and electrochemical responsiveness of boron-doped nanocrystalline diamond thin-film electrodes, Chemistry of Materials 15 (2003) 879.
[4] A.E. Fischer, Y. Show, G.M. Swain, Electrochemical performance of diamond thin-film electrodes from different commercial sources, Analytical Chemistry 76 (2004) 2553.
[5] J.A. Bennett, J. Wang, Y. Show, G.M. Swain, Effect of sp^2-bonded nondiamond carbon impurity on the response of boron-doped polycrystalline diamond thin-film electrodes, Journal of the Electrochemical Society 151 (2004) E306.
[6] S. Wang, V.M. Swope, J.E. Butler, T. Feygelson, G.M. Swain, The structural and electrochemical properties of boron-doped nanocrystalline diamond thin-film electrodes grown from Ar-rich and H_2-rich source gases, Diamond and Related Materials 18 (2009) 669.
[7] I. Duo, A. Fujishima, C. Comninellis, Electron transfer kinetics on composite diamond (sp^3)-graphite (sp^2) electrodes, Electrochemistry Communications 5 (2003) 695.
[8] J. Hees, R. Hoffmann, A. Kriele, W. Smirnov, H. Obloh, K. Glorer, B. Raynor, R. Driad, N. Yang, O.A. Williams, C.E. Nebel, Nanocrystalline diamond nanoelectrode arrays and ensembles, ACS Nano 5 (2011) 3339.
[9] S. Ernst, L. Aldous, R.G. Compton, The electrochemical reduction of oxygen at boron-doped diamond and glassy carbon electrodes: a comparative study in a room-temperature ionic liquid, Journal of Electroanalytical Chemistry 663 (2011) 108.
[10] R.D. Rogers, K.R. Seddon, Ionic liquids – solvents of the future? Science 302 (2003) 792.
[11] J.L. Anderson, D.W. Armstrong, G-T. Wei, Ionic liquids in analytical chemistry, Analytical Chemistry 78 (2006) 2893.
[12] V.I. Parvulescu, C. Hardacre, Catalysis in ionic liquids, Chemical Reviews 107 (2007) 2615.
[13] P. Hapiot, C. Lagrost, Electrochemical reactivity in room-temperature ionic liquids, Chemical Reviews 108 (2008) 2238.
[14] H. Tokuda, K. Hayamizu, K. Ishii, M.A.B.H. Susan, M. Watanabe, Physicochemical properties and structures of room temperature ionic liquids. 1. Variation of anionic species, Journal of Physical Chemistry B 108 (2004) 16593.
[15] L.E. Barrosse-Antle, A.M. Bond, R.G. Compton, A.M. O'Mahony, E.I. Rogers, D.S. Silvester, Voltammetry in room temperature ionic liquids: comparisons and contrasts with conventional electrochemical solvents, Chemistry – An Asian Journal 5 (2010) 202.
[16] A. Balducci, U. Bardi, S. Caporali, M. Mastragostino, F. Soavi, Ionic liquids for hybrid supercapacitors, Electrochemistry Communications 6 (2004) 566.
[17] V.R. Koch, L.A. Dominey, C. Nanjundiah, M.J. Ondrechen, The intrinsic anodic stability of several anions comprising solvent free ionic liquids, Journal of the Electrochemical Society 143 (1996) 798.
[18] T. Tsuda, C.L. Hussey, Electrochemical applications of room-temperature ionic liquids, The Electrochemical Society Interface 16 (2007) 42.
[19] D-Y. Kim, J. Wang, J. Yang, H-Y. Kim, G.M. Swain, Electrolyte and temperature effects on the electron transfer kinetics of $Fe(CN)_6^{3-/4-}$ at boron-doped diamond thin film electrodes, Journal of Physical Chemistry C 115 (2011) 10026.
[20] Y. Lauw, M.D. Horne, T. Rodopoulos, F.A.M. Leermakers, Room-temperature ionic liquids: excluded volume and ion polarizability effects in the electrical double-layer structure and capacitance, Physical Review Letters 103 (2009) 117801.
[21] A.A. Kornyshev, Double-layer in ionic liquids: paradigm change? Journal of Physical Chemistry B 111 (2007) 5545.
[22] S. Baldelli, Surface structure at the ionic liquid–electrified metal interface, Accounts of Chemical Research 41 (2008) 421.
[23] C. Zhao, G. Burrell, A.A.J. Torriero, F. Separovic, N.F. Dunlop, D.R. MacFarlane, A.M. Bond, Electrochemistry of room temperature protic ionic liquids, Journal of Physical Chemistry B 112 (2008) 6923.
[24] M.T. Alam, M.M. Islam, T. Okajima, T. Ohsaka, Capacitance measurements in a series of room-temperature ionic liquids at glassy carbon and gold electrode interfaces, Journal of Physical Chemistry C 112 (2008) 16600.
[25] N. Fietkau, A.D. Clegg, R.G. Evans, C. Villagrán, C. Hardacre, R.G. Compton, Electrochemical rate constants in room temperature ionic liquids: the oxidation of a series of ferrocene derivatives, ChemPhysChem 7 (2006) 1041.
[26] N. Tachikawa, Y. Katayama, T. Miura, Electrode kinetics of ferrocenium/ferrocene in some amide-based room-temperature ionic liquids physical and analytical electrochemistry, Electrochemical and Solid-State Letters 12 (11) (2009) F39.
[27] C. Lagrost, D. Carrié, M. Vaultier, P. Hapiot, Reactivities of some electrogenerated organic cation radicals in room-temperature ionic liquids: toward an alternative to volatile organic solvents? Journal of Physical Chemistry A 107 (2003) 745.
[28] M.A. Islam, M.T. Alam, T. Okajima, T. Ohsaka, Electrical double layer structure in ionic liquids: an understanding of the unusual capacitance–potential curve at a nonmetallic electrode, Journal of Physical Chemistry C 113 (2009) 3386.
[29] H. Liu, G. Zhu, The electrochemical capacitance of nanoporous carbons in aqueous and ionic liquids, Journal of Power Sources 171 (2007) 1054.
[30] H. Liu, P. He, Z. Li, Y. Liu, J. Li, L. Zheng, J. Li, The inherent capacitive behavior of imidazolium-based room-temperature ionic liquids at carbon paste electrode general topics, Electrochemical and Solid-State Letters 8 (2005) J17.
[31] M.C. Granger, G.M. Swain, The influence of surface interactions on the reversibility of ferri/ferrocyanide at boron doped diamond thin film electrodes articles, Journal of the Electrochemical Society 146 (1999) 4551.
[32] S. Haymond, G.T. Babcock, G.M. Swain, Electron transfer kinetics of ferrocene at microcrystalline boron-doped diamond electrodes: effect of solvent and electrolyte, Electroanalysis 15 (2003) 249.
[33] S. Ranganathan, T-C. Kuo, R.L. McCreery, Facile preparation of active glassy carbon electrodes with activated carbon and organic solvents, Analytical Chemistry 71 (1999) 3574.
[34] L.E. Barrosse-Antle, L. Aldous, C. Hardacre, A.M. Bond, R.G. Compton, Dissolved argon changes the rate of diffusion in room temperature ionic liquids: effect of the presence and absence of argon and nitrogen on the voltammetry of ferrocene, Journal of Physical Chemistry C 113 (2009) 7750.
[35] R.S. Nicholson, I. Shain, Theory of stationary electrode polarography. Single scan and cyclic methods applied to reversible, irreversible, and kinetic systems, Analytical Chemistry 36 (1964) 706.
[36] R.S. Nicholson, Theory and application of cyclic voltammetry for measurement of electrode reaction kinetics, Analytical Chemistry 37 (1965) 1351.
[37] A.J. Bard, L.R. Faulkner (Eds.), Electrochemical Methods: Fundamentals and Applications, 2nd ed., John Wiley & Sons, New York, 2001.
[38] R.E. Panzer, P.J. Elving, Behavior of carbon electrodes in aqueous and nonaqueous systems, Journal of the Electrochemical Society 119 (1972) 864.
[39] R.A. Marcus, On the theory of electron transfer reactions. VI. Unified treatment for homogeneous and electrode reactions, Journal of Chemical Physics 43 (1965) 679.

[40] R.A. Marcus, Electron transfer at electrodes and in solution: comparison of theory and experiment, Electrochimica Acta 13 (1968) 995.
[41] R.J. White, H.S. White, A random walk through electron-transfer kinetics, Analytical Chemistry 77 (2005) 214A.
[42] K.B. Holt, A.J. Bard, Y. Show, G.M. Swain, Scanning electrochemical microscopy and conductive probe atomic force microscopy studies of hydrogen-terminated boron-doped diamond electrodes with different doping levels, Journal of Physical Chemistry B 108 (2004) 15117.
[43] S. Wang, G.M. Swain, Spatially heterogeneous electrical and electrochemical properties of hydrogen-terminated boron-doped nanocrystalline diamond thin film deposited from an Argon-rich $CH_4/H_2/Ar/B_2H_6$ source gas mixture, Journal of Physical Chemistry C 111 (2007) 3986.
[44] H.V. Patten, K.E. Meadows, L.A. Hutton, J.G. Iacobini, D. Batistel, K. McKelvey, A.W. Colburn, M.E. Newton, J.V. Macpherson, P.R. Unwin, Electrochemical mapping reveals direct correlation between heterogeneous electron-transfer kinetics and local density of states in diamond electrodes, Angewandte Chemie International Edition 51 (2012) 7002.
[45] L. Xiao, E.J.F. Dickinson, G.G. Wildgoose, R.G. Compton, A comparison of electron transfer kinetics of three common carbon electrode surfaces in acetonitrile and in room temperature ionic liquid 1-butyl-3-methylimidiazonium hexafluorophosphate: correlation to surface structure and the limit of the diffusion domain approximation, Electroanalysis 22 (2010) 269.